Flow of groundwater with variable density and viscosity, Atikokan Research Area, Canada

Duke U. Ophori

Abstract Flow of groundwater with variable density and viscosity was simulated at the Atikokan Research Area (ARA) in northwestern Ontario, Canada. An empirical viscosity–concentration equation was modified to include total-dissolved-solids (TDS) data from the ARA. The resulting equation was used successfully to estimate reasonably accurate viscosity values over the expected range of temperature and concentration, in comparison with experimental values derived for sodium chloride solutions. A three-dimensional finite-element code, MOTIF, developed by Atomic Energy of Canada Limited, was used in the simulations. The inclusion of the effects of depth-increasing temperature and TDS-dependent fluid-density distribution, while maintaining only a temperature-dependent viscosity relationship in a simulation, resulted in a more penetrative flow against expected buoyancy effects (i.e., the physics of the system was not honored). Accounting for concentration in the viscosity equation caused water to be less penetrative and more in accordance with the expected physics of the system. A conclusion is that fluid concentration should be considered simultaneously in calculating the density and viscosity of a fluid during modeling of variable-density flow in areas underlain by fluids with high TDS. Results of simulations suggest that both flow directions and magnitudes should be employed simultaneously during the calibration of a model. Large-scale groundwater movement in the ARA may be analyzed with carefully selected vertical no-flow boundaries. By incorporating the geothermal temperature gradient, groundwater recharge increases by 12%; thus, this gradient plays a significant role in groundwater flow at the ARA. Variability in the fluid concentration at the ARA neither decreases nor increases recharge into the groundwater system. The hypothesis that an isolated continuous regional flow system may exist at depth in the ARA is not supported by these simulations.

Résumé Un écoulement souterrain à densité et à viscosité variables a été simulé sur le site expérimental d'Atikokan, dans le nord-ouest de l'Ontario (Canada). Une équation empirique liant la viscosité à la concentration a été modifiée pour prendre en compte les données de minéralisation de l'eau, en provenance de ce site. L'équation résultante a été appliquée avec succès à l'estimation avec une précision acceptable des valeurs de viscosité dans la gamme concernée de température et de concentration, par comparaison avec des valeurs expérimentales fournies par des solutions de chlorure de sodium. Un modèle 3D aux éléments finis, MOTIF, développé par Atomic Energy of Canada Limited, a servi à la modélisation. La prise en considération des effets de la distribution du fluide en fonction de sa densité du fait de l'augmentation de la température avec la profondeur et de sa minéralisation, tout en gardant uniquement une relation entre la viscosité et la température dans la simulation, a abouti à un écoulement plus pénétrant par rapport aux effets attendus de densité (c'est-à-dire que la physique du système n'est pas respectée). La prise en compte de la concentration dans l'équation de viscosité fait que l'eau pénètre moins, ce qui est plus en accord avec la physique prévue pour le système.

Il faut en conclure que la concentration du fluide doit intervenir à la fois dans le calcul de la densité et dans celui de la viscosité d'un fluide pour la modélisation d'un écoulement dû à des densités variables dans des zones situées sous des fluides à forte minéralisation. Les résultats des simulations laissent supposer que les directions d'écoulement et les ordres de grandeur doivent être utilisés en même temps lors de la calibration du modèle.

Les mouvements de l'eau souterraine à large échelle dans le site expérimental peuvent être analysés à partir de limites choisies convenablement sans écoulement vertical. En introduisant le gradient géothermique, la recharge de la nappe augmente de 12%; par conséquent ce gradient joue un rôle significatif dans l'écoule-

Received, September 1996
Revised, September 1997, February 1998
Accepted, February 1998

Duke U. Ophori
Department of Earth and Environmental Studies,
Montclair State University, Upper Montclair, NJ 07043, USA
Fax: +1-973-655-4390
e-mail: ophorid@pegasus.montclair.edu

ment souterrain du site. La variabilité de la concentration du fluide dans le site ni ne décroît, ni n'augmente la recharge de la nappe. L'hypothèse qu'un système aquifère régional continu et isolé existe en profondeur sur le site n'est pas confirmée par les simulations.

Resumen Se simuló el flujo de agua subterránea con densidad y viscosidad variables en el Atikokan Research Area (ARA) al noroeste de Ontario, Canadá. Se modificó una ecuación empírica de relación entre concentración y viscosidad para incluir los datos de Total de Sólidos Disueltos (TSD) en el ARA. La ecuación resultante se usó para estimar con razonable precisión los valores de viscosidad en el rango esperado de temperaturas y concentraciones, comparándolos con los valores experimentales derivados de disoluciones de cloruro sódico. En las simulaciones se utilizó un programa de elementos finitos tridimensionales, MOTIF, desarrollado por la Atomic Energy of Canada Limited. El incluir en las simulaciones los efectos de temperatura creciente en profundidad y de densidad variable en función del TSD, mientras se mantiene una relación de viscosidad dependiente únicamente de la temperatura, da lugar a un flujo mucho más penetrante frente a los efectos de flotación esperados (es decir, contradiciendo la física del sistema). Al tener en cuenta la concentración en la ecuación de viscosidad se produce un flujo menos penetrante, mucho más de acuerdo con la física del propio sistema.

Como conclusión, la concentración del fluido se ha de tener en cuenta cuando se modele la densidad y viscosidad de un fluido con densidad variable en áreas con gran contenido de TSD. Las simulaciones sugieren que las direcciones y magnitudes del flujo se deben usar simultáneamente durante la calibración de un modelo de densidad variable.

El flujo de agua subterránea a gran escala en el ARA se puede analizar seleccionando cuidadosamente contornos verticales de flujo nulo. Al incorporar el gradiente geotérmico, la recarga se incrementa en un 12%; por tanto, este gradiente tiene un papel destacado en el flujo subterráneo en el ARA. La variabilidad en la concentración del fluido en esta misma zona no produce ninguna variación en la recarga al sistema. Las simulaciones contradicen la hipótesis de que exista un flujo regional correspondiente al de un sistema aislado en el ARA.

Key words Canada · waste disposal · numerical modeling · groundwater density/viscosity

Introduction

Atomic Energy of Canada Limited (AECL), through the Canadian Nuclear Fuel Waste Management Program (CNFWMP), is currently assessing the concept of disposing nuclear-fuel waste in a vault 500–1000 m deep within plutonic rocks in the Canadian Shield. AECL is using field data obtained from investigations of specific research areas on the Canadian Shield to develop representative models for the rock or geosphere. Field data have been collected since the late 1970s in the Atikokan Research Area (ARA) of northwestern Ontario (Davison et al. 1994a,b). Among other properties, this area contains groundwater of highly variable total dissolved solids (TDS), ranging from fresh water at the surface, brackish and saline waters at depths below 500 m, to brines at depths of about 2000 m. A hypothesis is that the TDS might cause enough variation in fluid density and viscosity to affect groundwater flow and contaminant transport through the region. A knowledge of these effects is necessary to evaluate alternative conceptual models. Numerical modeling of groundwater flow and solute transport is an efficient method for assessing the extent of these effects. Most contaminant-transport models assume that free convection due to the density of the solute is negligible relative to forced advection by hydraulic gradients and dispersion. The works of researchers such as Cambarnous and Bories (1975), Schincariol and Schwartz (1990), Hayworth et al. (1991), Dane et al. (1991), Nield and Bejan (1992), and Hassanizadeh and Leijnse (1995) show that this assumption is valid only for contaminant plumes of low concentrations and not for highly concentrated leachates. In the ARA, where highly concentrated brines have been sampled, density effects are of potential significance.

Several studies have considered the effects of density variations on groundwater flow without similarly considering viscosity variations (e.g., Fried 1975; Singh and Stammers 1989; and Koch and Zhang 1991, 1992). Koch and Zhang (1992) recognize that a small viscosity change $\partial\mu$ of 5% results in a 5% change in total velocity, and they argue that such a small variation in velocity is completely masked by other uncertainties in the physical and numerical model. Larger viscosity changes could be generated by saline waters and brines of the type in the ARA.

Kestin and Wang (1957) and Kestin et al. (1958) show that the viscosity and density of a fluid are closely coupled. A potential exists, therefore, to produce incorrect flow patterns in simulations in which variable density is considered along with a constant viscosity. Accordingly, variations in both density and viscosity in relation to concentration have been considered in studies such as INTERA (1981), Garven and Freeze (1984a,b), Herbert et al. (1988), Welty and Gelhar (1992), and Evans and Raffensperger (1992). These studies, however, do not discuss the significance of considering the density–concentration relationship independently of the viscosity–concentration relationship during flow modeling.

In this study, a viscosity–concentration (TDS) relationship was generated based on Robinson and Stokes' (1965) equation and on field total-dissolved-solids data from the ARA. Using a three-dimensional finite-ele-

ment code, MOTIF, variable-density groundwater flow was simulated at the ARA with and without the concentration-dependent viscosity expressions.

The Conceptual Model

Field geologic studies at the ARA indicate that fracturing is intense in a background rock mass with major fracture zones of relatively high permeability (Davison et al. 1994a). The frequency of occurrence of the major fracture zones is low, and the zones can be effectively treated as discrete high-permeability planes embedded in the background equivalent porous medium. The modeled region, shown in *Figure 1*, covers an area of about 4000 km^2 north of the town of Atikokan, Ontario, Canada, and was selected to coincide with sufficiently large groundwater divides and valleys that are believed to provide no-flow boundary conditions. Field geological, geophysical, geochemical, hydrological, and hydrogeological mapping have aided in simplifying the geology. The rock mass is intersected by three sets of fractured zones that strike northeast–southwest (NE–SW), north–south (N–S), and northwest–southeast (NW–SE). Major fracture zones included in the simulations are shown in the model grid of *Figure 2*. Mapping revealed that the fracture zones are vertical. Available data indicate that the fracture zones have larger permeability values than does the rock mass, and that seven permeability layers with values decreasing linearly with depth may be used to represent both fracture zones and rock mass. The permeabilities and porosities used in the study were varied between simulations, and their values are discussed along with the different simulations.

For non-isothermal fluid flow, neglecting pressure, the fluid density, ρ (kg/m^3), is described by the polynomial:

$$\rho = \rho_o (1 + [T - T_o]\,[A + (T - T_o)\,B] + \varepsilon C) \quad (1)$$

where ρ_o = reference density = 1000 kg/m^3 (Weast 1971), T_o = reference temperature = 6 °C, and ε = constant coefficient of density variability with concentration (in moles/liter) = 3.09×10^{-3} in the ARA.

The coefficients A and B have been determined to have values of -3.17×10^{-4} °C^{-1} and -2.56×10^{-6} °C^{-2} by curve fitting to experimental data (Forsythe 1964).

Fluid viscosity, μ (Pa.s), is often described by the Guzman–Andrade equation (Perry and Chilton 1973):

$$\mu(T) = A_1 \exp[B_1/(273 + T)] \quad (2)$$

where the coefficients A_1 and B_1 have been determined to have values of 1.98404×10^{-6} Pa.s and 1.82585×10^3 °C, respectively, by curve fitting to experimental data (Forsythe 1964).

The conceptual model presented herein is only one of various possible interpretations based on available data. It has been constructed to allow sensitivity analyses with respect to assumptions about features and their properties, as described in a later section.

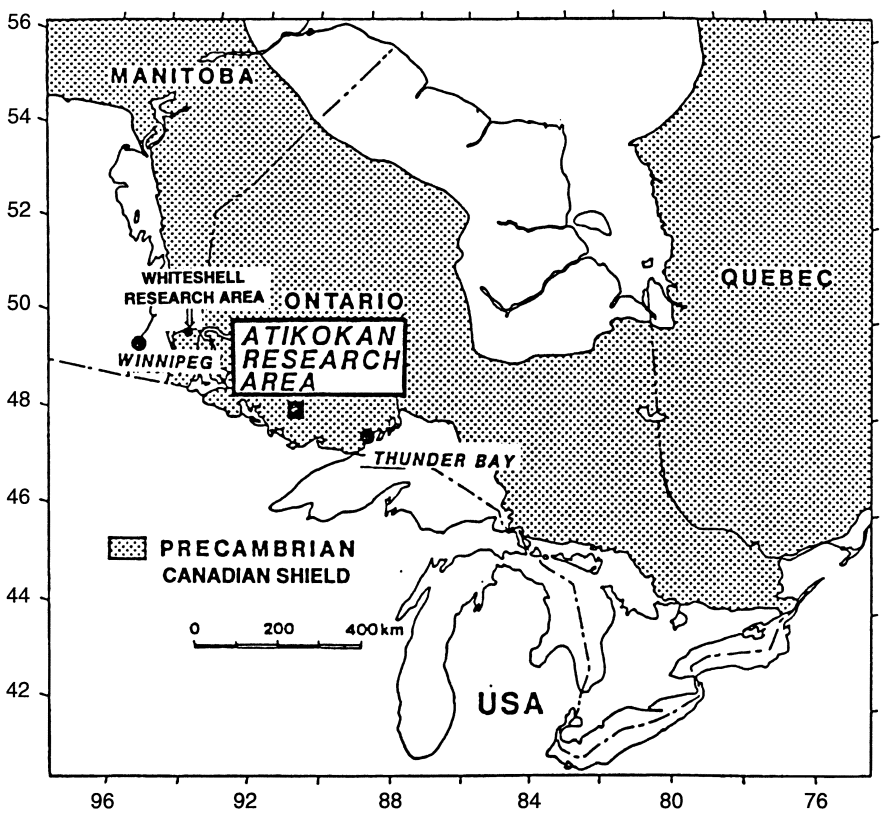

Fig. 1 Location of the Atikokan Research Area, Ontario, Canada

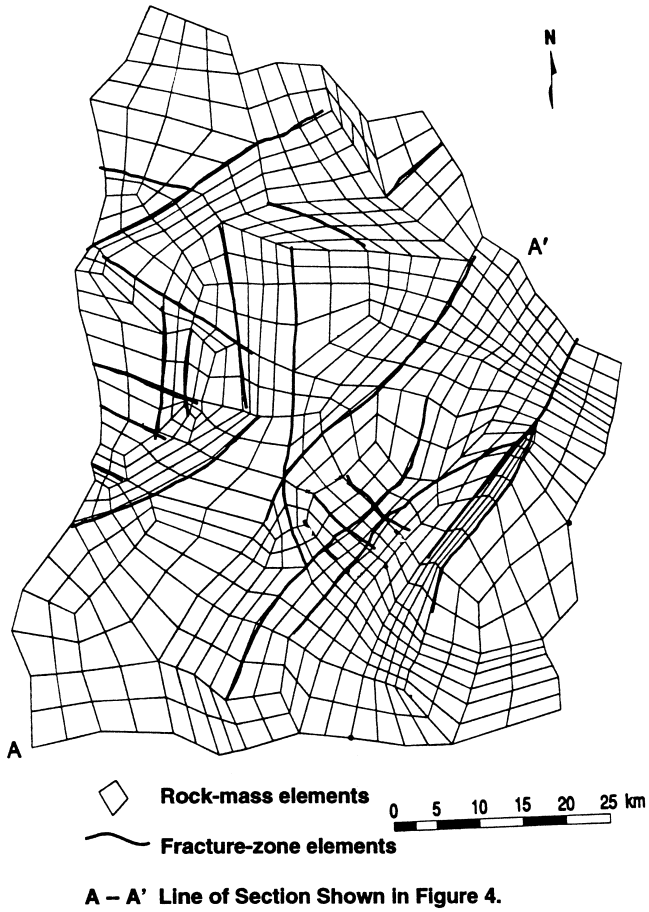

Fig. 2 Plan view of the finite-element mesh. Section A–A' is a straight line between A and A'

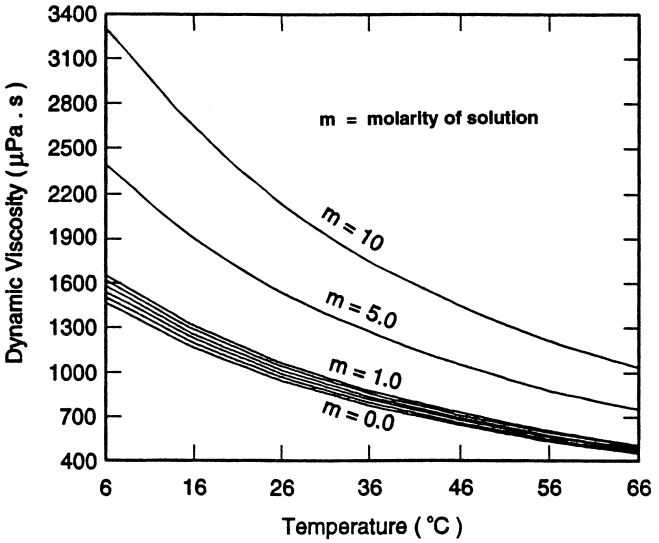

Fig. 3 Relation between viscosity and temperature for various TDS concentrations at the ARA at 1 MPa

Equations of State for the ARA

Fluid density and viscosity can vary significantly with temperature (T) and salinity (C), and to a lesser degree with pressure (P) in regions with fluids of high TDS. The influences of temperature and concentration on fluid density are commonly known as the thermohaline convection process. In most numerical modeling studies, the equation of state for density (ρ) includes a consideration of concentration, as in Eq. (1). Viscosity (μ), on the other hand, is often assumed to be constant or as a function of temperature (T) only, as in Eq. (2).

Because brackish and saline waters and brines exist in the ARA, both density and viscosity are allowed to vary with concentration (i.e., with TDS). However, detailed experimental data pertinent to the generation of a viscosity–TDS relationship for the ARA are not available; neither are such data collected routinely in most groundwater studies. The empirical approach described in Appendix A was used to obtain the following viscosity–concentration (TDS) relationship for flow modeling at the ARA:

$$\mu(T,C) = \mu(T,0) \times (1 + 0.005\sqrt{C_{TDS}} + 0.1223\, C_{TDS}) \quad (3)$$

where C_{TDS} is the concentration of TDS in moles/liter, and μ (T,C) is the viscosity of solution at temperature T and concentration C.

The viscosity values generated with Eq. (3) for the expected TDS range in the ARA are shown in *Figure 3*. These values compare well with those that were estimated by Garven and Freeze (1984a,b) for sodium chloride solutions.

Spatially Variable Density and Viscosity

Field observations at the ARA reveal that TDS contents vary substantially in space. TDS ranges from about zero at the ground surface to saturation values that are about 300,000 mg/L at a depth of about 2000 m (Fritz and Frape 1982; Gascoyne et al. 1987). This range in TDS is enough to cause spatial variations in density that might influence groundwater flow. Therefore, the effects of density variation on flow should be analyzed, in order to improve predictions of contaminant transport at the ARA.

The observed distribution of TDS and, thus, the distribution of density, also raises several questions about the origin of groundwater at the research area. A knowledge of the origin of the groundwater is needed to establish boundary conditions necessary for flow modeling.

Two alternative origins for the saline groundwater have been proposed (Fritz and Frape 1982): (1) the chemical composition of these waters resulted solely from rock–water interactions; and (2) the saline waters are the remnants of ancient seawater that underwent secondary rock–water interaction through time, which thereby altered its chemical composition to that in existence today. The first proposition, supported by many

researchers (e.g., Kamineni et al. 1992), indicates that all the waters (including those at depth) are meteoric and are, therefore, recharged and discharged through the ground surface. Acceptance of this proposition implies that vertical no-flow boundaries below major groundwater divides and valleys may be appropriate for modeling, on the basis of flow symmetry at such locations. However, if these groundwater basins are self-contained in accordance with the first proposition, several questions need to be addressed: (1) Where are the points of discharge of the brines and saline waters at the surface? and (2) Is mineral precipitation followed by mixing and dilution adequate to mask the discharge of brines at the surface? Whereas this condition might well be valid, it is not unreasonable, at least on a conceptual basis, to conceive of a deep-flow system of brines and saline waters on which a more active shallow system of fresh and brackish water is superimposed. This hypothesis is in agreement with the second origin of brines and saline water proposed above. In this case, vertical no-flow boundaries may be modified during modeling to accommodate inflow or outflow of water. By adjusting the flow boundaries to account for the two proposed origins, uncertainties regarding the choice of an adequate size of the regional domain for modeling purposes are simultaneously reduced.

In this section, the effects of variable density on groundwater flow at the ARA are analyzed. Sensitivity tests of several parameters that specify the fractured porous-medium system, including the boundary conditions, are carried out. A realistic scenario is established that can be used as a reference case when selecting a more detailed local model.

Simulations

Simulations of regional groundwater flow in the ARA were performed using the three-dimensional finite-element code, MOTIF (Guvanasen 1984; Chan et al. 1987). MOTIF was developed to perform analyses of groundwater flow, heat, and solute/radionuclide transport in fractured rocks. It can be used to analyze variable saturated flow in regions with solid matrix and discrete fractures (fracture zones). The solid matrix is represented by hexahedral eight-noded elements, whereas fractures and small flow conduits are represented by four-noded quadrilateral planar elements and two-noded linear elements, respectively. In this study, the fracture zones were considered to be equivalent porous media; thus, they were simulated with eight-noded solid elements. MOTIF has been tested over the years by comparison with experimental and analytical data, and with other programs (Davison et al. 1994a; Chan et al. 1995; Makurat et al. 1995; Rutqvist et al. 1996). Details of the equations solved by the MOTIF code are discussed in Davison et al. (1994a).

A representation of the conceptual model of the ARA by a finite-element mesh (see *Fig. 2*) has 20 vertical layers of elements and, in all, consists of 17,160 elements and 15,981 nodes. Only steady-state conditions were considered in this study. The MOTIF code is well designed to use the Galerkin weighted-residual finite-element formulation and the Picard iterative scheme to handle this problem. Despite this special design, numerical problems were observed in the solution of the transport problem. These problems were overcome by adjusting certain model parameters and performing many simulations until the required convergence was obtained. Although all the simulations were performed in three dimensions, the results are discussed with reference to the section A–A' of flow vectors, taken along the maximum hydraulic gradient and located as shown in *Figure 2*.

The fracture zones have permeabilities that are one to two orders of magnitude greater than that of the rock mass. The permeabilities decrease with depth from 10^{-11} m^2 and 10^{-12} m^2 for the fracture zones and rock mass at the surface, respectively, to a minimum value of 10^{-21} m^2 for both fracture zones and rock mass. Porosity was also one to two orders of magnitude greater in the fracture zones and decreased with depth from 0.1 and 0.011 at the surface for the fracture zones and rock mass, respectively, to a minimum of 0.0025. In most of the simulations, the vertical and bottom boundaries of the model were assumed to be no-flow and impermeable. The water table, assumed to coincide with the surface topography, was specified to generate the flow. For the solute and heat transport, concentration and temperature were specified at the top and bottom boundaries, and zero flux was used at all the vertical boundaries. Concentration and temperature are presumed to affect the simulated groundwater flow through variable density and viscosity. Variations in these general conditions were made in the following case simulations, and their effects were analyzed.

Base Case: Constant Density and Viscosity

A base-case simulation was made with which the results of subsequent runs were compared. The conditions of this base-case run are the same as described in the preceding section, except that fresh water was assumed to occupy the entire domain under isothermal conditions of 6 °C. Thus, a constant fluid density of 1000 kg/m^3 and viscosity of 1.472×10^{-3} Pa.s were used.

About 16 local, 3 intermediate, and one regional system are shown in *Figure 4*. Flow is mainly active in the shallow local systems relative to the intermediate and regional systems, which occur at depths greater than 2000 m below the surface.

A water balance was calculated for the model in which the annual recharge, which equals discharge at steady state, was determined to be 70.9 mm. The average flow through each of the 20 layers of the system was also estimated. *Table 1* shows that this flow decreases with depth, because of decreasing permeability with depth and because losses occur due to natural discharge from every depth level in the system.

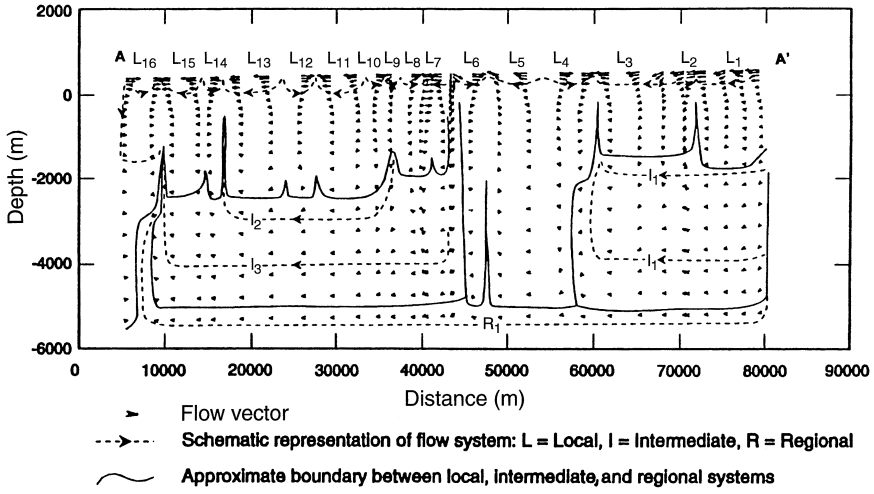

Fig. 4 Flow vectors along section A–A' for base-case run. Maximum length of vector plotted represents maximum velocity magnitude of 1319 m/a; velocity range plotted is $0–10^4$ m/a; vector lengths are in log scale. Line of section is shown in *Figure 2*

Case 1: Geothermal Temperatures

Case 1 was conducted to analyze the effects on flow of variable density, as determined by geothermal temperatures. During this simulation, the geothermal-temperature (T) distribution, as calculated with the MOTIF code (Ophori and Chan 1996), was specified to control the fluid density and viscosity as in Eqs. (1) and (2). All other conditions of this simulation are the same as for the base case.

The simulated flow patterns of case 1 and the base case (*Fig. 4*) are essentially the same. *Table 1* shows, however, that annual recharge into the system increases from 70.9 to 78 mm (i.e., by 12% under the conditions of geothermal temperatures). In addition, flow through each depth layer increases in proportion to the increase in temperature. Thus, recharged water penetrates deeper into the system as a consequence of decreased viscosity caused by the increase in temperature and consequent increase in hydraulic conductivity.

Case 2: Concentration-Dependent Density and Concentration-Independent Viscosity

In addition to the conditions of case 1, variable density was added to case 2 through the TDS distribution. Gascoyne (1991) describes the observed TDS distribution in the ARA with the equation:

$$\log \mathrm{TDS} = 2.13 + 0.002\mathrm{d} \qquad (4)$$

where d equals depth below ground surface (m).

Table 1 Vertical Darcy flux through model layers. The flux through layer 1 is the average annual basin recharge

Layer	Vertical Darcy flux, in mm/yr							
	Base Case	Case 1	Case 2	Case 3	Case 4	Case 5	Case 6	Case 7
1	7.1×10^{1}	7.8×10^{1}	7.8×10^{1}	7.8×10^{1}	7.8×10^{1}	7.8×10^{1}	3.3×10^{0}	1.5×10^{0}
2	2.3×10^{0}	2.5×10^{0}	2.5×10^{0}	2.5×10^{0}	2.5×10^{0}	2.5×10^{0}	5.7×10^{-2}	8.1×10^{-2}
3	2.0×10^{-1}	2.2×10^{-1}	2.2×10^{-1}	2.2×10^{-1}	2.2×10^{-1}	2.2×10^{-1}	3.9×10^{-3}	5.5×10^{-3}
4	7.1×10^{-2}	8.4×10^{-2}	8.4×10^{-2}	8.4×10^{-2}	8.4×10^{-2}	8.3×10^{-2}	2.4×10^{-3}	3.2×10^{-3}
5	2.3×10^{-3}	2.8×10^{-3}	2.8×10^{-3}	2.8×10^{-3}	2.9×10^{-3}	2.6×10^{-3}	1.5×10^{-4}	1.6×10^{-4}
6	5.3×10^{-4}	6.8×10^{-4}	6.9×10^{-4}	6.8×10^{-4}	7.3×10^{-4}	6.6×10^{-4}	1.3×10^{-4}	1.2×10^{-4}
7	1.0×10^{-4}	1.4×10^{-4}	1.5×10^{-4}	1.4×10^{-4}	1.6×10^{-4}	1.4×10^{-4}	1.3×10^{-4}	1.3×10^{-4}
8	2.9×10^{-5}	4.0×10^{-5}	4.4×10^{-5}	4.0×10^{-5}	5.4×10^{-5}	4.7×10^{-5}	1.3×10^{-4}	1.4×10^{-4}
9	9.0×10^{-6}	1.4×10^{-5}	1.6×10^{-5}	1.3×10^{-5}	3.1×10^{-5}	2.6×10^{-5}	1.4×10^{-4}	1.4×10^{-4}
10	2.7×10^{-6}	4.3×10^{-6}	6.5×10^{-6}	4.1×10^{-6}	3.3×10^{-5}	2.9×10^{-5}	3.4×10^{-5}	3.9×10^{-5}
11	1.2×10^{-6}	2.2×10^{-6}	3.8×10^{-6}	2.0×10^{-6}	3.8×10^{-5}	3.3×10^{-5}	4.1×10^{-5}	4.8×10^{-5}
12	7.5×10^{-7}	1.5×10^{-6}	2.9×10^{-6}	1.4×10^{-6}	1.5×10^{-6}	1.1×10^{-6}	8.3×10^{-7}	1.2×10^{-6}
13	5.6×10^{-7}	1.2×10^{-6}	2.3×10^{-6}	1.1×10^{-6}	8.2×10^{-7}	7.3×10^{-7}	5.2×10^{-7}	4.8×10^{-7}
14	4.0×10^{-7}	9.0×10^{-7}	1.7×10^{-6}	8.1×10^{-7}	6.8×10^{-7}	6.3×10^{-7}	5.1×10^{-7}	4.5×10^{-7}
15	3.0×10^{-7}	7.0×10^{-7}	1.3×10^{-6}	6.2×10^{-7}	5.7×10^{-7}	5.5×10^{-7}	6.5×10^{-7}	5.2×10^{-7}
16	2.2×10^{-7}	5.3×10^{-7}	1.0×10^{-6}	4.8×10^{-7}	4.8×10^{-7}	4.6×10^{-7}	8.4×10^{-7}	5.2×10^{-7}
17	1.5×10^{-7}	4.0×10^{-7}	7.6×10^{-7}	3.5×10^{-7}	4.8×10^{-7}	5.1×10^{-7}	8.6×10^{-7}	6.7×10^{-7}
18	1.0×10^{-7}	2.9×10^{-7}	5.5×10^{-7}	2.5×10^{-7}	6.4×10^{-7}	6.5×10^{-7}	1.1×10^{-6}	7.5×10^{-7}
19	6.2×10^{-8}	1.8×10^{-7}	3.4×10^{-7}	1.6×10^{-7}	9.8×10^{-7}	9.8×10^{-7}	1.3×10^{-6}	1.1×10^{-6}
20	2.1×10^{-8}	5.9×10^{-8}	1.2×10^{-7}	5.4×10^{-8}	2.6×10^{-6}	2.6×10^{-6}	2.9×10^{-6}	2.8×10^{-6}

Once the TDS has been calculated with Eq. (4), the density, ρ, at any point in the system, with respect to temperature (T) and concentration (C or TDS) but ignoring pressure, is estimated by Eq. (1). Concentration-independent viscosity was specified by using Eq. (2).

The flow pattern that results from case 2 is similar in terms of flow-system numbers and flow directions to the patterns of the base case and case 1. However, a significant difference occurs in the magnitudes of flow. *Table 1* indicates that although the same quantity of water is recharged into the system at the surface in cases 1 and 2, more water flows through layer 6 and deeper layers in case 2 than in case 1. That is, water is more "penetrative" to depths in case 2. This observation is contrary to expectation, because TDS and, thus, density, increases with depth and buoyancy therefore would be expected to render the water less penetrative. A detailed explanation of this observation is given by Ophori (1998).

Case 3: Concentration-Dependent Viscosity

Following the case 2 simulation, the viscosity Eq. (2) was modified to include the effects of concentration (in the form of TDS), as in Eq. (3). Eq. (1) is the density equation that was used in this simulation.

As with the preceding runs, the flow pattern obtained from this simulation is essentially unchanged. *Table 1* shows that the effect of increasing density with depth is a less penetrative fluid flow through deep layers in the system relative to the case 1 flow, in which density was not considered to vary with TDS. The buoyancy physics of the flow system appear to be reasonably simulated. The results of this simulation suggest that, for modeling purposes, both the density and viscosity of a fluid need to be correctly estimated in terms of temperature and concentration. This conclusion is similar to that of Ophori (1998), that even fluids with a range of TDS similar to that of seawater must be correctly accounted for in density and viscosity for accurate modeling results. The preceding modeling exercise also reveals that comparison of flow patterns alone is not sufficient for model calibration, but that the comparison of flow patterns should be supplemented with analysis of flow magnitudes. A similar conclusion regarding the effects of density on groundwater flow is provided by Franke and Reilly (1987).

Boundary Conditions and Geologic Framework

This portion of the study was prompted by the lack of an appropriate description of the adequate size of the region that should be considered for both the regional-scale and proposed more local-scale analysis at the ARA. The vertical boundaries of the preceding models have been assumed to be no-flow boundaries on the basis of their coincidence with valleys and groundwater divides. However, flow may occur through such boundaries. Sensitivity analyses performed on these boundaries test the effects of possible flow across them. The set-up for this analysis also tests the possibility of a separate flow system at depth, above which shallow flow systems occur. The existence or non-existence of fracture zones in the system was also evaluated through the following simulation cases.

Case 4: Flow Through Vertical Boundaries

Case 4 simulation was designed to analyze the effects of flow through the vertical boundaries of the ARA. The conditions of simulation are the same as those of case 3, except that horizontal flow was allowed across the vertical boundaries. To create horizontal flow, hydrostatic pressure conditions were specified along the vertical boundaries from a depth of 700 m to the bottom of the model, as shown in *Figure 5*. The hydrostatic pressure in this depth range was converted to the equivalent fresh-water head and specified at the corresponding nodes according to the fluid density at the nodes. The depth of 700 m corresponds to the level at which saline water begins to occur in the system. The use of hydrostatic-pressure conditions to simulate horizontal flow is discussed by Segol et al. (1975), Orr and Kreitler

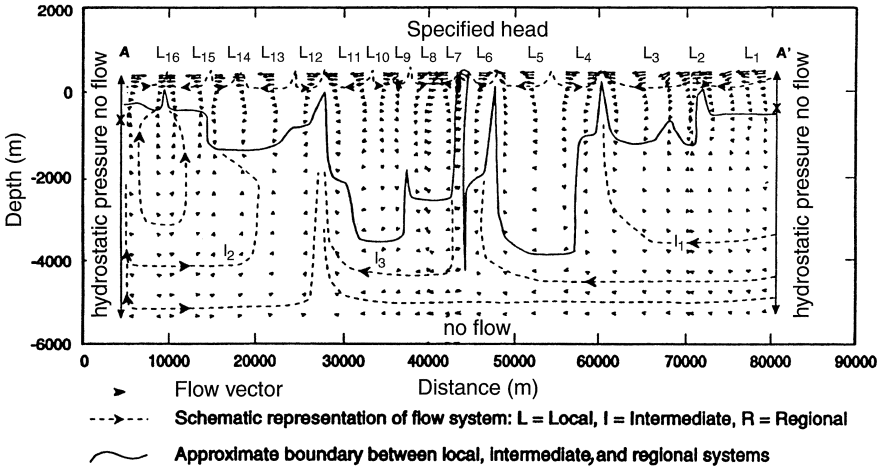

Fig. 5 Specified boundary conditions and flow vectors along section A–A' for case 4. Maximum length of vector plotted represents maximum velocity magnitude of 1427 m/a; velocity range plotted is $0–10^4$ m/a; and vector lengths are in log scale. Line of section is shown in *Figure 2*

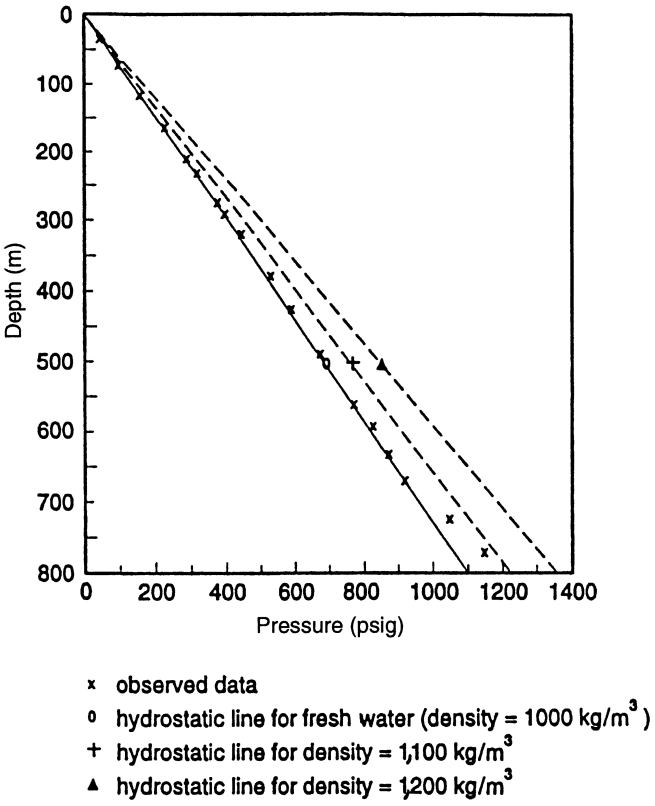

Fig. 6 Typical pressure–depth curves in the Whiteshell Research Area, Ontario, Canada

(1985), and Senger and Fogg (1990a,b). In this study, the hydrostatic-pressure conditions were used because most of the boreholes drilled in the Whiteshell Research Area of the Canadian Shield (*Fig. 1*) show pressure–depth curves that are essentially hydrostatic, as shown in *Figure 6*. No-flow conditions were specified along the vertical boundaries in the depth range of 0–700 m (*Fig. 5*). The bottom horizontal boundary was treated as impermeable, and the top boundary condition was considered to be the surface topography, as with earlier simulations. The density and viscosity are described with Eqs. (1) and (3), respectively.

Comparison of *Figures 4* and *5* shows that the use of hydrostatic-pressure vertical-boundary conditions allows water to flow into the system through the right boundary. Some water also flows out of the system through the left boundary. The sixteen shallow local flow systems are maintained in both figures, but the intermediate and regional systems are significantly altered in direction. However, the alteration of the intermediate systems is restricted to stretches of one-third of the domain to the left and right of *Figure 5*. Flow in the middle one-third of the domain between the X-distances of 30,000–60,000 m is unaltered. This condition probably results from a strong topographic control of the flow in the middle third of the domain. The topography possesses enough gravitational energy to drive flow from the surface to the bottom of the modeled area in the mid-regions. In addition, the high-permeability fracture zones simulated herein probably contribute to driving the flow from the surface to great depths. The effects of the specified surface topography and fracture zones are analyzed in a later section. However, a conclusion is that the conditions of this simulation produce results that do not support the hypothesis of a continuous deep regional flow system on which smaller local systems are superimposed near the surface. Horizontal flow through the vertical boundaries may not be regionally continuous along lengths as great as considered in this study (about 70,000 m).

Table 1 shows that recharge and discharge through the surface of the model are essentially the same as those of case 3, suggesting that horizontal inflow into the model at depth does not hinder recharge from the surface. However, observation of the flow pattern (*Fig. 5*) indicates that water recharged from the surface may mix with that recharged at depth before being discharged at either the surface or out from the system across vertical boundaries at depth. Flow across the top five layers is the same as in case 3, but horizontal flow alters the vertical flow magnitudes from the sixth layer, at a depth of 500 m, to the bottom of the model.

Case 5: Removal of Fracture Zones

In case 4, the occurrence of vertical fracture zones of higher permeability may have preferentially channeled flow vertically to and from the surface to distort the hypothesized continuous regional flow system at depth. Case 5 was designed to evaluate the effects of removal of the fracture zones from the conceptual model. The permeabilities of the fracture zones were changed to attain the same values as the rock mass. All other parameters are the same as in case 4. Results of this simulation show that the flow pattern is essentially the same with or without the fracture zones (*Fig. 5*). No regional flow system develops, and flow in the mid-regions is still driven to the bottom of the model by the surface topography. This result is evidence that the surface topography in the ARA plays a dominant role in defining the flow pattern. The removal of the fracture zones, however, reduces vertical flow magnitudes significantly at depth, although recharge into the top surface layer remains essentially unaffected (*Table 1*).

Case 6: Flat Topography

Following the simulation of case 5, the effect of topography was removed from the analysis in case 6 by specifying an average hydraulic head of 450 m at every node along the surface (top) boundary. No fracture zones were simulated. *Figure 7* shows that convection cells develop due to inflow and outflow from the vertical boundaries and probably to the buoyancy effects of density. Such cells cause recharge and discharge conditions near the surface. Although inflow from the vertical boundaries penetrates deeper into the system than

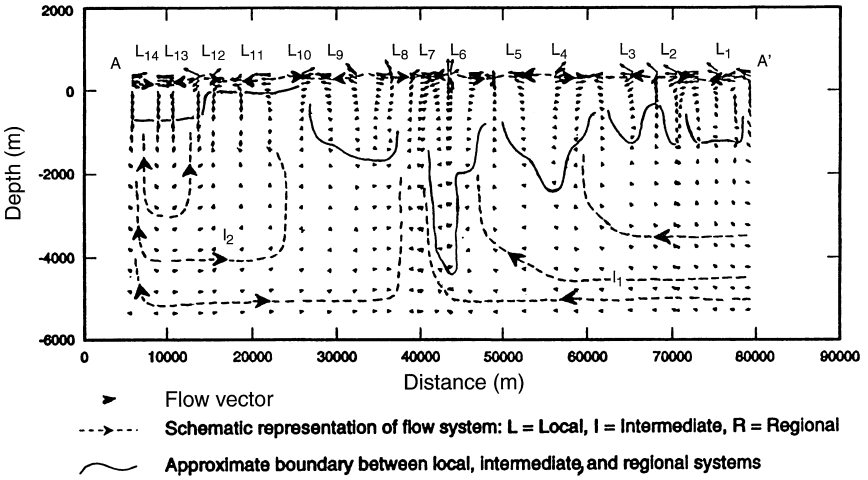

Fig. 7 Flow vectors along section A–A' for case 6. Maximum length of vector plotted represents maximum velocity magnitude of 7.7 m/a; velocity range plotted is 0–10 m/a; vector lengths are in log scale. Line of section is shown in *Figure 2*

in case 5, no continuous deep regional flow system exists across the entire domain. *Table 1* indicates that the convection cells cause some recharge and discharge of water at the surface. The recharge rate is approximately 5% of the quantity that would be recharged under the actual topographic relief.

Case 7: Flat Topography and Fracture Zones

In case 7, the conditions of case 6 were retained, except that fracture zones were simulated with greater permeability. This arrangement was intended to test the influence of the fracture zones on the flow pattern under conditions of a flat surface topography.

This simulation produced a flow pattern similar to that in *Figure 7*, indicating that the geologic framework does not influence the flow directions to a significant degree in the ARA. *Table 1* does show, however, that flow magnitudes at depth are increased by the presence of the fracture zones.

Summary and Conclusions

The effects of spatially variable density on groundwater flow in the ARA was studied using the MOTIF finite-element code. In a base-case simulation with fresh water under isothermal conditions of 6 °C, a flow pattern was generated that consists of 16 local, three intermediate, and one regional flow systems. Variation of fluid density and viscosity with the geothermal temperature gradient produced a flow pattern that is similar in configuration to the fresh-water pattern, but recharge and flow through the system increased in magnitude by about 12%. TDS-dependent changes in flow were insignificant relative to temperature-dependent changes. When concentration was specified to increase fluid density with depth while viscosity was made independent of concentration, greater flow occurred through the system than in the case in which concentration was not considered. This result is contrary to expectation based on the buoyancy physics of the system. When both density and viscosity were simulated to vary appropriately with concentration, less flow occurred through the system than in the case without concentration, as expected from the buoyancy forces. Thus, density and viscosity variations should be considered carefully in modeling variable-density flow of groundwater.

The hypothesis that a large, continuous, saline, regional flow system may underlie the fresh-water local systems at the ARA was tested by opening the vertical boundaries of the model to flow, using hydrostatic boundary conditions. Results show that such a regional system probably does not exist. The topographic relief has a strong influence that drives the flow to great depths in relatively smaller local and intermediate systems. Due to their vertical orientation, the fracture zones increase the magnitudes of recharge and flow through the region, but they do not change the configuration of the flow pattern, which is controlled primarily by the strong topographic control.

References

Combarnous MA, Bories SA (1975) Hydrothermal convection in saturated porous media. In: Chow Ven Te (ed) Advances in hydroscience. Academic Press, New York, pp 231–307

Chan T, Reid KJA, Guvanasen V (1987) Numerical modeling of coupled fluid, heat and solute transport in deformable fractured rock. In: Coupled processes associated with nuclear waste repositories. Proc Int Symp, Berkeley, CA, pp 605–625

Chan T, Khair K, Jing L, Ahola M, Noorishad J, Vuillod E (1995) International comparison of coupled thermo-hydro-mechanical models of a multiple-fracture bench-mark problem: DECOVALEX Phase I, Bench Test 2. Int J Rock Mech Min Sci Geomech Abstr 32:435–452

Dane JH, Guven O, Oostrom M, Hayworth JS (1991) Stability and mixing of dense aqueous phase plumes in porous media. EOS Trans Am Geophys Union 72:126

Davison CC, Chan T, Brown A, Gascoyne M, Kamineni DC, Lodha GS, Melnyk TW, Nakka BW, O'Connor PA, Ophori DU, Scheier NW, Soonawala NM, Stanchell FW, Stevenson DR, Thorne GA, Vandergraaf TT, Vilks P, Whitaker SH (1994a) The disposal of Canada's nuclear fuel waste: The geosphere model for post-closure assessment. Atomic Energy of Canada Limited Report, AECL-10719, COG-93–9, Pinawa, Manitoba, Canada

Davison CC, Brown A, Everitt RA, Gascoyne M, Kozak ET, Lodha GS, Martin CD, Soonawala NM, Stevenson DR, Thorne GA, Whitaker SH (1994b) Site screening and evaluation technology for disposal of Canada's nuclear fuel waste. Atomic Energy of Canada Limited Report, AECL-10713, COG-93–3, Pinawa, Manitoba, Canada

Evans DG, Raffensperger JP (1992) On the stream function for variable-density groundwater flow. Water Resour Res 28:2141–2145

Forsythe WE (1964) Smithsonian physical tables, 9th edn, revised. Smithsonian Institution, Washington, DC

Franke OL, Reilly, TE (1987) The effects of boundary conditions on the steady-state response of three hypothetical groundwater systems: Results and implications of numerical experiments. US Geological Survey Water Supply Paper, 2315 pp

Fried JJ (1975) Groundwater pollution. Elsevier Science, New York

Fritz P, Frape, SK (1982) Saline groundwaters in the Canadian Shield: a first review. Chem Geol 36:179–190

Garven G, Freeze, RA (1984a) Theoretical analysis of the role of groundwater flow in the genesis of stratabound ore deposits, 1. Mathematical and numerical model. Am J Sci 284:1085–1124

Garven G, Freeze, RA (1984b) Theoretical analysis of the role of groundwater flow in the genesis of stratabound ore deposits. 2. Quantitative results. Am J Sci 284:1125–1174

Gascoyne M (1991) Hydrogeochemical data for the Atikokan geosphere model. Memorandum AGB-91-304, Atomic Energy of Canada Limited, Pinawa, Manitoba, Canada

Gascoyne M, Davison CC, Ross JD, Pearson R (1987) Saline groundwater and brines in plutons in the Canadian Shield. In: Fritz P, Frape SK (eds) Saline water and gases in crystalline rocks. Geol Assoc Can Spec Pap 33:53–68

Guvanasen V (1984) Development of a finite-element hydrogeological code and its application to geoscience research. In: Proc 17th Information Meeting of the Nuclear Fuel Waste Management Program, vol 2, pp 554–566

Hassanizadeh MS, Leijnse A (1995) A non-linear theory of high-concentration-gradient dispersion in porous media. Adv Water Resour 18:203–215

Hayworth JS, Guven O, Dane JH, Oostrom M (1991) Experimental studies of dense solute plumes in porous media. EOS Trans Am Geophys Union 72:130

Herbert AW, Jackson CP, Lever DA (1988) Coupled groundwater flow and solute transport with fluid density strongly dependent on concentration. Water Resour Res 24:1781–1795

INTERA Environmental Consultants, Inc (1981) Regional and room-scale hydrological simulations of the Atikokan site (Research Area 4). AECL, Whiteshell Laboratories, Pinawa, Manitoba, Canada, 57 pp

Kamineni DC, Gascoyne M, Melnyk TW, Frape SK, Blomquist P (1992) Cl and Br in mafic and ultramafic rocks: significance for the origin of salinity of groundwater. In: Kharaka YK, Maest AS (eds) Proc 7th Int Symp on Water–Rock Interaction WR-7, Park City, UT. AA Balkema, Rotterdam

Kestin J, Wang HE (1957) Corrections for the oscillating-disk viscometer, J App Mech Trans, ASME 79:197–206

Kestin J, Wang HE, Providence RI (1958) The viscosity of five gases: A re-evaluation. J App Mech, Trans ASME 80:11–17

Koch M, Zhang G (1991) Numerical simulation of the migration of density-dependent contaminant plumes, SCRI. Report to the Florida Department of Environmental Regulation, Florida State Univ, Tallahassee

Koch M, Zhang G (1992) Numerical simulation of the effects of variable density in a contaminant plume. Ground Water 30:731–742

Makurat A, Ahola M, Khair K, Noorishad J, Rosengren L, Rutqvist J (1995) The DECOVALEX test-case one. Int J Rock Mech Min Sci Geomech Abstr 32:399–408

Nield DA, Bejan A (1992) Convection in porous media. Springer, Berlin Heidelberg New York

Ophori DU (1996) Regional groundwater flow in the Atikokan Research Area: spatially variable density and viscosity, Atomic Energy of Canada Limited Report, AECL-11082, COG-93-184, Pinawa, Manitoba, Canada

Ophori DU (1998) The significance of viscosity in variable-density flow of groundwater. J Hydrol 204:261–270

Ophori DU, Chan T (1996) Regional groundwater flow in the Atikokan Research Area: Model development and calibration. Atomic Energy of Canada Limited Report, AECL-11081, COG-93-183, Pinawa, Manitoba, Canada

Orr ED, Kreitler CW (1985) Interpretation of pressure–depth data from confined underpressured aquifers exemplified by the Deep-Basin brine aquifer, Palo Duro Basin, Texas. Water Resour Res 21:533–544

Perry RH, Chilton GH (1973) Chemical engineer's handbook, 5th edn. McGraw-Hill, New York

Robinson RA, Stokes RH (1965) Electrolyte solutions, 2nd edn, revised. Butterworths, London

Rutqvist SF, Follin S, Khair K, Nguyen S, Wilcock P (1996) Experimental investigation and mathematical simulation of a borehole injection test in deformable rocks (TC6). In: Stephansson O, Jing L, Tsang CF (eds) Mathematical and experimental studies of coupled thermo-hydro-mechanical processes in fractured media. Elsevier, Amsterdam

Schincariol RA, Schwartz FW (1990) An experimental investigation of variable density flow and mixing in homogeneous and heterogeneous media. Water Resour Res 26:2317–2329

Segol G, Pinder GF, Gray WG (1975) A Galerkin finite-element technique for calculating the transient position of the saltwater front. Water Resour Res 11:343–347

Senger RK, Fogg GE (1990a) Stream functions and equivalent freshwater heads for modeling regional flow of variable-density groundwater, 1:Review of theory and verification. Water Resour Res 26:2089–2096

Senger RK, Fogg GE (1990b) Stream functions and equivalent freshwater heads for modeling regional flow of variable-density groundwater, 2:Application and implications for modeling strategy. Water Resour Res 26:2097–2106

Singh SP, Stammers WN (1989) A potential theory-based finite-element algorithm for freshwater recharge of saline aquifers: a sharp interface model. Water Resour Res 25:1685–1694

US National Research Council (1929) International critical tables of numerical data, physics, chemistry and technology, vol 5. McGraw-Hill, New York

Weast RC (ed) (1971) CRC Handbook of chemistry and physics, 52nd edn. Chemical Rubber Company, Cleveland

Welty C, Gelhar LW (1992) Simulation of large-scale transport of variable density and viscosity fluids using a stochastic mean model. Water Resour Res 28:815–827

Appendix A: Derivation of the Viscosity–Concentration Equation of State for the ARA

The Viscosity Equation

Because experimental data on viscosity are not routinely available, it is common practice to adopt well known empirical equations of state. Eq. (A1) was adopted and used in this study. Proposed by Robinson and Stokes (1965), this equation shows that viscosity dependence on concentration, ignoring pressure, may be expressed as:

$$\mu(T,C) = \mu(T,0) \times (1 + 0.005\sqrt{\Sigma C_i} + \Sigma D_i C_i) \qquad (A1)$$

where C_i is the concentration of dissolved ion (i) in moles/liter, D_i is the temperature-dependent coefficient

for each ion (i), and μ (T,C) is the viscosity of solution at temperature T and concentration C.

Two problems are encountered in applying Eq. (A1) to TDS: (1) the concentration C is in moles/liter requiring that a molecular weight be known for TDS; and (2) the coefficient D is known for some ions and not for TDS. It is necessary, therefore, to define a molecular weight and D for TDS. These parameters were obtained through the following averaging process.

Molecular Weight of TDS

The sum of the concentrations of individual ions is assumed to be equal to the concentration of TDS, and it is assumed that the combined TDS behaves like a homogeneous chemical species, i.e.,

$$C_{TDS} = \Sigma C_i \quad \text{(A2)}$$

where C_{TDS} is the concentration of TDS in water in moles/liter. The sum of the weights of individual ions is further assumed to be equal to the total weight of TDS. Then:

$$M_{TDS} \times C_{TDS} = \Sigma M_i C_i \quad \text{(A3)}$$

where M_{TDS} is the molecular weight of TDS, and M_i is the molecular weight of individual ions.

Therefore,

$$M_{TDS} = \Sigma M_i C_i / \Sigma C_i \quad \text{(A4)}$$

For each of 54 groundwater samples from the ARA, molecular weight was calculated with Eq. (A4). Using the molecular weights estimated for each sample, an average molecular weight of 53.65 g was calculated for TDS. Molarity was also estimated for the samples to range from 0.0008–1.072 mol/L. Further details of this calculation are reported by Ophori (1996).

The D Coefficient for TDS

The same assumptions used in the calculation of the average molecular weight were applied in the estimation of the D coefficient. Because D_i is temperature-dependent, the D equation is slightly different from Eq. (A4) and may be written as:

$$\{D_{TDS}\}_T = \Sigma < D_i >_T C_i / \Sigma C_i \quad \text{(A5)}$$

where $\{D_{TDS}\}_T$ is the coefficient D for TDS at temperature T.

For each sample, and for selected temperature values of 0, 10, 20, 30, 40, 50, and 60 °C (encompassing the expected temperature range at the ARA), the D coefficient was calculated for TDS with Eq. (A5). An average D coefficient of 0.1223 was calculated for the ARA.

The Viscosity–TDS Relationship

The derived viscosity–TDS relationship may now be written as:

$$\mu(T,C) = \mu(T,0) \times (1 + 0.005\sqrt{C_{TDS}} + 0.1223\, C_{TDS}) \quad \text{(A6)}$$

In this analysis, pressure is ignored, because dynamic viscosity does not vary significantly in the pressure range of 0.0–0.05 GPa (0–5 km depth) that is considered in this study (US National Research Council 1929).